Journal of Computational Electronics (2022) 21:1061–1069
https://doi.org/10.1007/s10825-022-01910-z

A first-principles investigation of electronic structure and ferromagnetic properties in alkali metal-doped ZnS/Se semiconductors

W. Adli[1] **· A. H. Belbachir**[1]

Received: 9 January 2022 / Accepted: 4 June 2022 / Published online: 2 July 2022

Abstract
The full potential linearized augmented plane wave based on density functional theory is carried out to study the magnetism and electronic structures of group I^A elements (K, Rb, Cs)-doped zinc blende ZnX (X = S, Se). Total energy calculations indicate that the ferromagnetic phase is always energetically more stable than the non-magnetic phase at equilibrium volume. All doped systems are half-metallic ferromagnets with gap in the majority spin channel. The energy band gap decreases on increasing the size of dopant atom from K to Cs. The magnetic moments are mainly carried by anions (S or Se) surrounding the dopant atom. The intrinsic ferromagnetism is originated from the partly filled anionic *p* orbitals, which is different from classical magnetic materials containing transition metal (TM) atoms. The absence of TM atoms makes these alloys interesting candidates for the study of half-metallic *p* electron ferromagnetism.

Keywords Density functional theory · Electronic properties · Half-metallic ferromagnets · *p*-electron ferromagnetism

1 Introduction

Spintronics, or spin-based electronics, which offers fascinating opportunities for a new generation of devices by exploiting the spin of electrons as well as their charge [1, 2] has attracted much attention over the past two decades. Half-metallic ferromagnets (HMFs), where one of the two spin channels is semiconducting (either spin-up or spin-down) and the other is metallic, are the most desirable components for the high-performance spintronic devices as they provide nearly 100% spin polarization at the Fermi level (E_F). In particular, diluted magnetic semiconductors (DMSs), fabricated by doping conventional compounds semiconductors with magnetic elements have triggered more research [3–6] aiming at finding materials that are HMFs. For practical device applications, the search for DMS exhibiting the ferromagnetism at or above room temperature (RT) is required. Since Dietl et al. [7] theoretically predicted that RT ferromagnetism could exist in GaN- and ZnO-based DMSs, extensive experimental and theoretical studies have been directed toward wide band gap semiconductors III-V and II-VI in searching for RT ferromagnetic DMS materials [8–15]. However, the literature shows that transition metals (TM) find lower solubility in III-V semiconductors, when compared to II-VI semiconductors [16]. In this respect, TM-doped II-VI (such as ZnO, ZnS, ZnSe, ZnTe, CdS, CdSe, etc.) compounds have remained a focus of great attention by various research groups. For instance, Sambasivam et al. found ferromagnetism at RT in Co/fe-doped ZnS [17, 18]. Lakshmi et al. studied magnetism in Mn: ZnS nanocrystalline and found room temperature ferromagnetism [19]. In the experimental study for Co-, Cr- and V-doped ZnO [20], the magnetization measurements showed that all the samples exhibited RT ferromagnetism. Also, the ferromagnetism behavior was observed experimentally in Cr-doped ZnTe [21, 22]. Soundararajan et al. [21] revealed ferromagnetism in $Zn_{1-x}Cr_xTe$ (x = 0.05) alloy powder with Curie temperature (T_C) much greater than RT. Hou et al. [22] obtained T_C of 365 K for Cr concentration > 0.18.

Although a large amount of the literature has been reported on the magnetism of TMs-doped DMSs, experimental works have produced inconsistent results and the mechanism of ferromagnetism of such systems is still under

✉ W. Adli
adli.phys@gmail.com

[1] Laboratoire d'Analyse et d'Application des Rayonnements, Département de Génie Physique, Faculté de Physique, Université des Sciences et de la Technologie d'Oran (USTO), BP1505 El-M'naouer, 31000 Oran, Algeria

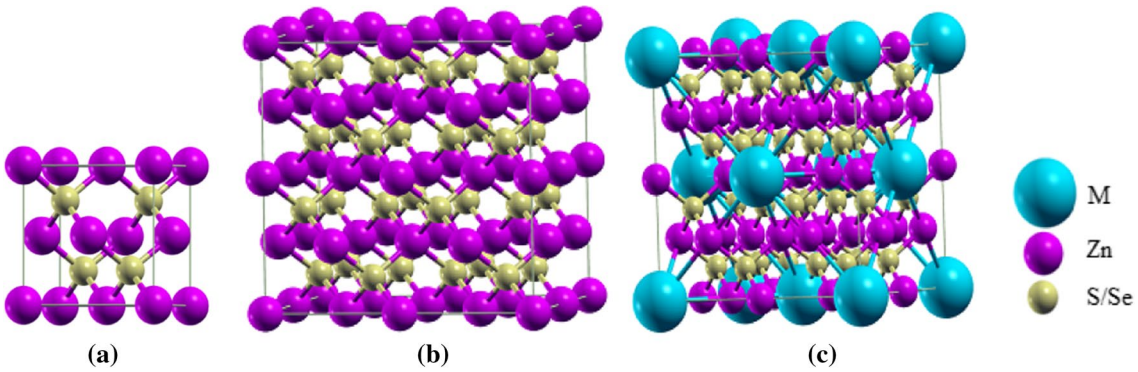

Fig. 1 Conventional cell of **a** ZnS/Se, **b** Zn_8 $(S/Se)_8$, **c** $Zn_{0.875}M_{0.125}S/Se$ (M = K, Rb, Cs) (Color figure online)

active debate. This because the TMs dopants often have a clustering tendency or secondary phase [23, 24] which are detrimental to applications of DMS. To overcome this drawback, a new class of DMS with intrinsic ferromagnetism behavior has been discovered through doping of non-magnetic atoms into the host semiconductors. This phenomenon is known in the literature with various names as d^0 ferromagnetism, p-electron ferromagnetism or sp-electron ferromagnetism. Several theoretical investigations have shown that appropriate non-magnetic elements substitutions in II-VI semiconductors like C-doped ZnO [25] and CdS [26], B/C/N-doped BeO [27] and CaO [28], Cu-doped ZnO [29], as well as K/Cu-doped MgS [30] can induce intrinsic ferromagnetism. On the other hand, experimental observation of RT ferromagnetism in Cu-, N- and C-doped ZnO [31–33] confirmed these theoretical predictions.

During last decade, the binary II–VI chalcogenides ZnS and ZnSe have received enormous research interests in the field of high performance optoelectronic devices due to their wide band gap. The both compounds crystallize in zinc blende structure (ZB) at an ambient pressure but can be also prepared with wurtzite structure. Though the ZnS/Se compounds are in the same family and have the same stable phase, their electronic properties (mainly band gap) are different from each other. Bulk zinc sulfide (ZnS), with a larger band gap of 3.68 eV [34], is an important candidate for ultraviolet light-emitting diodes (LEDs), solar cells, optical sensors, photocatalytic devices, etc. [35–38], whereas bulk zinc selenide (ZnSe), which has a band gap of ~ 2.8 eV, playing a striking role for application in energy upconversion [39]. Moreover, besides the mentioned properties of ZnS/Se compounds, new functionality can be added to these materials by means of introducing magnetic degree of freedom [40, 41].

These works motivated us to study the possibility of HM ferromagnetism in ZnX (X = S, Se) with group I^A elements (K, Rb, Cs) as dopants, searching for further HMFs that do not contain TM elements. Therefore, in the present paper we investigate the electronic and magnetic properties of these alloys in their ordered ZB structure by using first-principles density functional calculations. The roles played by alkali dopants and chalcogen atoms in ferromagnetic properties are discussed in order to establish the DMSs characteristics. The paper is structured as follows. The methodology is described in Sect. 2, while results and discussions are presented in Sect. 3. Finally, the concluding remarks are drawn in Sect. 4.

2 Computational method

The present calculations are performed by using the accurate full potential linearized augmented plane wave (FP-LAPW) method as incorporated in the wien2K package [42] within the framework of density functional theory (DFT) [43]. The generalized gradient approximation (GGA) parameterized by Perdew, Burke and Ernzerhof (PBE) [44] is used for the exchange and correlation potential.

The un-doped cells ZnS and ZnSe have zinc blende (B_3) structure with space group of 216 $\left(F\bar{4}3m\right)$, where the Zn atom is located at (0, 0, 0) and S/Se atom at (0.25, 0.25, 0.25) position (Fig. 1a). To simulate our doped systems ZnMX (M = K, Rb, Cs; X = S, Se), we have constructed cubic supercell Zn_8X_8 with 2 × 2 × 2 dimension, which contains 8 Zn and 8 (S/Se)atoms (Fig. 1b). For 12.5% doping concentration of M atom, the Zn atom positioned at (0, 0, 0) in supercell Zn_8X_8 is replaced by M atom forming the ternary alloy $Zn_{0.875}M_{0.125}X$, as shown in Fig. 1c.

To reach an appropriate degree of convergence, the cutoff parameter R_{MT} K_{max} is taken as 8.0, where R_{MT} is the smallest muffin-tin radius and K_{max} is the maximum modulus for the reciprocal lattice vectors. Inside the atomic spheres, the maximum value of angular momentum for the wave function expansion is l = 10. The fully relativistic and scalar relativistic approach is used for core and valence electrons,

respectively. Muffin-tin radii (R_{MT}) are chosen to be 2.0 bohr for S, 2.2 bohr for K, 2.4 bohr for Cs and 2.3 bohr for other atoms. For geometry optimization and physical property calculation, the Brillouin zone is sampled by Monkhorst–Pack mesh [45] of $5\times5\times5$ k-points. In our calculations, the atomic coordinates are fully relaxed until the maximum force acted on each atom is smaller than 2.10^{-3}Ry/a.u., and the self-consistent convergence of the total energy is set to 10^{-5} Ry/cell.

3 Results and discussions

The stability of the materials is one step forward to get insight into their physical properties. In this paper, the stability of studied DMS compounds has been estimated from the variation of total energy with respect to cell volume in both non-magnetic (NM) and ferromagnetic (FM) states. The equilibrium lattice constant (a), bulk modulus (B), its pressure derivative (B') and the total energy difference between NM and FM states $\left(\Delta E = E_{NM} - E_{FM}\right)$ at their equilibrium lattice constants are listed in Table 1. These predicted results have been obtained by fitting the calculated total energies as function of volume using Murnaghan's equation of state (EOS) [46]. This EOS describes the relationship between the variables (E, V) and it is given by

$$E(V) = E_0 + \frac{BV}{B'}\left[\frac{\left(V_0/V\right)^{B'}}{B'-1} + 1\right] - \frac{BV_0}{B'-1} \tag{1}$$

where V_0 is volume at zero pressure (i.e., equilibrium volume), V is the volume at pressure P and E_0 is the energy corresponding to the V_0. The B and B' can be calculated from the following formula:

$$B = -V\frac{\partial P}{\partial V} = V\left(\frac{\partial^2 E}{\partial V^2}\right)_{V_0} \tag{2}$$

$$B' = \left(\frac{\partial B}{\partial P}\right)_{P=0} \tag{3}$$

Our calculated lattice parameters increased from K- to Cs-doped ZnS/Se, which can be attributed to the increase in atomic radii. For all the six compounds, the FM state is more favorable in energy than the corresponding NM state. To evaluate the structural stability, the cohesive energy is introduced to make easy a comparison of stability of compounds. The cohesive energy of a solid is defined as the energy required to decompose it into single atoms, which is a measure of bonds strength. We calculated the cohesive energy of each compound using relation [47]

$$E_{coh}^{ZnMS/Se} = 2\left(E_{total}^{ZnMS/Se} - lE_{iso}^{Zn} - mE_{iso}^{M} - nE_{iso}^{S/Se}\right)/(l+m+n) \tag{4}$$

where $E_{coh}^{ZnMS/Se}$ refers to the total energy of the ZnMS/Se compounds, E_{iso}^{Zn}, E_{iso}^{M} and $E_{iso}^{S/Se}$ are the energies of an isolated Zn, M and S/Se atoms, respectively. l, m and n are the number of each atom in the unit cell. The cohesive energy versus

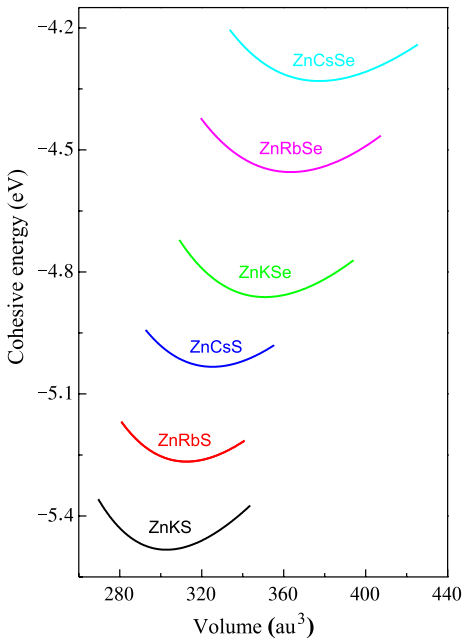

Fig. 2 Spin-polarized cohesive energy versus volume plot of ZnMS/Se (M = K, Rb, Cs) (Color figure online)

Table 1 Optimized parameters under non-magnetic (NM) and ferromagnetic (FM) order as well as total energy difference ΔE (meV/cell) for each case of M-doped ZnX

Compounds	FM ordering			NM ordering			ΔE (meV)
	a (Å)	B (Gpa)	B′	a (Å)	B (Gpa)	B′	
$Zn_{0.875}K_{0.125}S$	5.6414	56.3666	5.8097	5.6406	56.0754	5.7753	62.9819
$Zn_{0.875}Rb_{0.125}S$	5.7025	51.6796	5.5525	5.7009	51.8674	5.3481	64.0549
$Zn_{0.875}Cs_{0.125}S$	5.7797	48.3589	4.8160	5.7769	48.7891	4.7458	44.6500
$Zn_{0.875}K_{0.125}Se$	5.9271	45.5039	4.6220	5.9248	46.4879	4.2221	48.8093
$Zn_{0.875}Rb_{0.125}Se$	5.9932	44.4677	4.5694	5.9945	43.6824	3.9441	61.1778
$Zn_{0.875}Cs_{0.125}Se$	6.0826	41.5597	3.9517	6.0702	40.8092	3.5891	19.9039

volume curves under FM order are displayed in Fig. 2. For the sake of simplicity, we have presented the cohesive energy plots for only FM ground state. Figure 2 shows that absolute value of cohesive energy decreases as the doped elements range from K to Cs, which suggest that the stability of the alloys decreases with increasing dopant size which is consistent with decreasing bulks modulus given in Table 1.

The calculated total magnetic moment in all investigated compounds is exactly 1.00 μ_B, which are typical HM ferromagnets. It is well known that the HM ferromagnets with large magnetic moment are expected to present large stray magnetic fields, and thus lead to considerable energy losses in spintronic devices applications [48]. Thus, to this respect, a very interesting case is HM magnets which possess small values of magnetic moment. The total and atomic resolved magnetic moments of the alkali-doped ZnX (X = S, Se) at their equilibrium constants are summarized in Table 2. As indicated in the results, the total magnetic moment is principally contributed by doping atom M, its nearest neighboring X atoms and the interstitial region. However, the other farther X atoms and Zn atoms have vanishing moments. Summing up the magnetic moments, we found more than 62% of all magnetic moments are restricted within MX_4 tetrahedron in the doped systems. To obtain the visual impression of the magnetic property of the studied alloys, we have selected Rb-doped ZnS as an example for analysis of its three dimensional (3D) isosurface of spin charge density. This is shown in Fig. 3, where the spin density is localized mainly on the nearest neighboring S atoms, which derives from the *p* orbital. Although the magnetic moment induced by Rb atoms is small, it activates the *p* electrons of its connecting S atoms which contribute chiefly to the total moment. Thus alkali metals (K, Rb and Cs) behave as spin polarizers in host matrices.

The spin-polarized electronic structures of ZnMS/Se systems have been calculated. In the following, we concentrate the discussion on the computational electronic structure of ZnRbS/Se for which the magnetic stability is highest, while ZnKS/Se and ZnCsS/Se have similar behavior. Figure 4 shows the spin-polarized band structure of ZnRbS/

Table 2 Calculated total magnetic moment (m^{total}), local magnetic moments of Zn atom (m^{Zn}), doping atom (m^{M}), its nearest neighboring X atom $\left(m^{S_1/Se_1}\right)$ and other X atom $\left(m^{S_2/Se_2}\right)$, and interstitial magnetic moment $\left(m^{interstitial}\right)$ for each case of M-doped ZnX

Compounds	m^{Zn} (μ_B)	M^{M} (μ_B)	m^{S_1/Se_1} (μ_B)	m^{S_2/Se_2} (μ_B)	$m^{interstitial}$ (μ_B)	m^{total} (μ_B)
$Zn_{0.875}K_{0.125}S$	0.003	0.025	0.148	0.008	0.326	1.000
$Zn_{0.875}Rb_{0.125}S$	0.002	0.034	0.150	0.006	0.326	1.000
$Zn_{0.875}Cs_{0.125}S$	0.001	0.061	0.149	0.003	0.323	1.000
$Zn_{0.875}K_{0.125}Se$	0.002	0.022	0.157	0.010	0.298	1.000
$Zn_{0.875}Rb_{0.125}Se$	0.001	0.033	0.164	0.007	0.276	1.000
$Zn_{0.875}Cs_{0.125}Se$	0.001	0.053	0.165	0.005	0.275	1.001

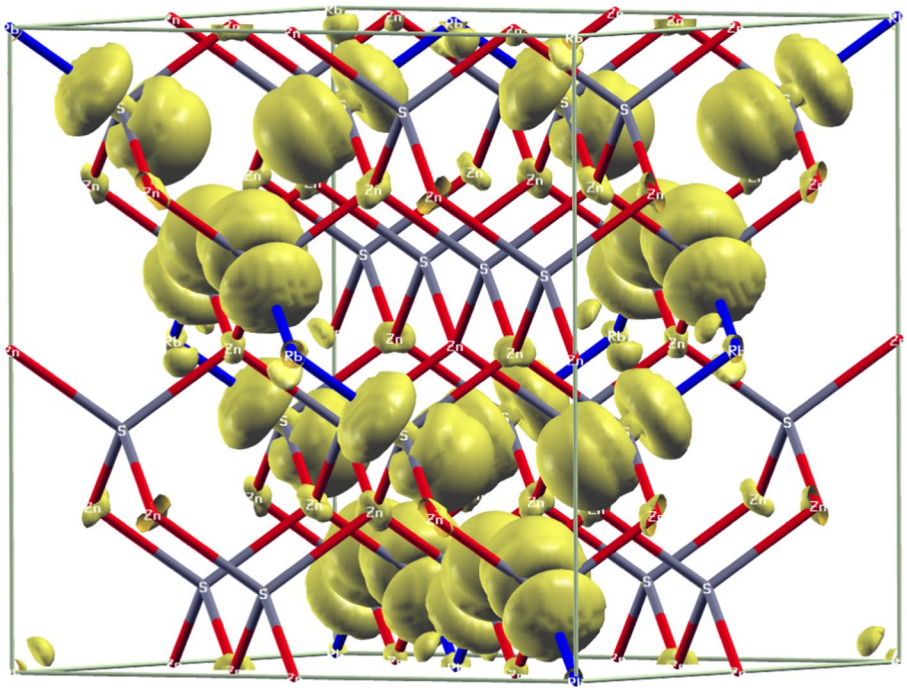

Fig. 3 A 3D isosurface of the spin charge density $(\rho = \rho_{up} - \rho_{down})$ for ZnRbS. The isosurface value of ρ (in yellow) is 0.013 e/A^3. The Zn, S and Rb atoms are represented by red, gray and blue colors, respectively (Color figure online)

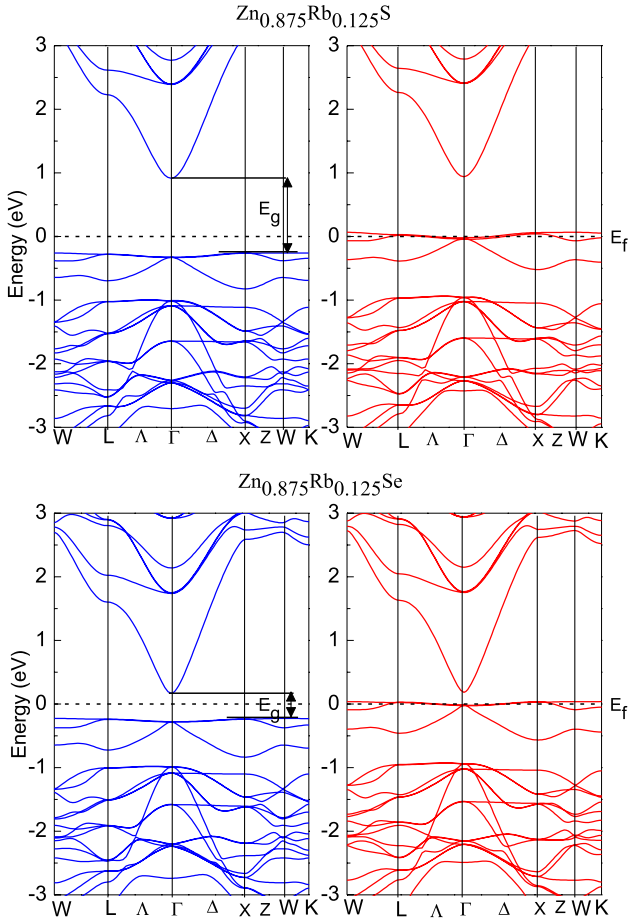

Fig. 4 Spin-polarized band structures of $Zn_{0.875}Rb_{0.125}S/Se$. The solid blue (red) lines represent the majority (minority) spin channel, and horizontal dashed line indicates Fermi level. The indirect band gaps are indicated by black arrows (Color figure online)

Se alloys for minority spin (spin-down) and majority spin (spin-up) configurations along high-symmetry directions in the first Brillouin zone. The minority spin channels are metallic whereas the majority spin channels keep semiconductor behavior with an indirect energy gap (E_g) of about 1.18 eV and 0.4 eV for ZnRbS and ZnRbSe, respectively. Therefore, these systems are HMFs, leading to 100% carrier spin polarization at the Fermi level (E_f). This is opposite to the properties of HMFs CrS [49] and V- and Cr-doped zinc chalcogenides [50], where the majority spin electrons exhibit metallic character and the energy gap is at the minority spin channel. The bands close to E_F in the whole Brillouin zone for both compounds and both spin channels are flat and nearly dispersionless. The main contributor to the flat band is chalcogen *p*-states. It has been argued by other authors [51, 52] that the mechanism leading to this phenomenon is an important condition for stability of HM ferromagnetism. Above flat band, the lower conduction band is shifted toward the Fermi level as we move along the I^A column from K to

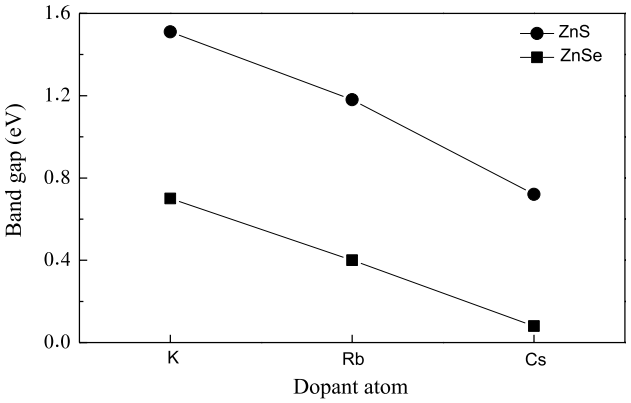

Fig. 5 Calculated band gap of ZnMS/Se (M = K, Rb, Cs) as a function of alkali dopant

Cs, and hence, the band gap decreases as shown in Fig. 5. Band gap is also found to decrease as one goes from S to Se atom.

The ternary compound under investigation does not contain TM atoms thus the proposed mechanism of magnetism is different from the Zener's *p–d* hybridization [53], the Zener's double exchange [54], the super-exchange [55] and the Ruderman–Kittel–Kasuya–Yoshida (RKKY) [56] mechanisms. To elucidate the mechanism which may be responsible for observed magnetic behavior in these systems, the total density of states (DOS) and partial DOS of the rubidium atom and one of its four nearest neighboring chalcogen atoms (S, Se) are calculated and illustrated in Figs. 6 and 7. From total DOS (TDOS) plots, we can see that spin splitting near the Fermi level shifts the spin-up states downward and spin-down states upward to lower the total energy of systems. The asymmetrical distributions of TDOS between spin-up and spin-down channels suggest the magnetism of such doped systems (see Figs. 6a and 7a). The partial DOS (PDOS) for each compound shows existing gaps in both spin directions that separate the anion and cation orbitals. The states below the gaps arise exclusively from (S, Se)-*p* orbitals, while the states above the gaps are of Rb-*d* orbitals (see Figs. 6b–c and 7b–c). As it is well known that for ZB structure, the tetrahedral crystal field splits the cation *d* states into threefold degenerate t_{2g} (d_{xy}, d_{xz} and d_{yz}) and twofold degenerate e_g $(d_{x^2-y^2}$ and $d_{z^2})$ symmetry states, as presented in Figs. 6d and 7d, while anions *p* states have t_{2g} symmetry. Only cation t_{2g} states can couple with the surrounding anions *p* orbitals having the same symmetry and create bonding and antibonding hybrid orbitals. The bands around E_f are composed mostly from S-3p/Se-4p states, hybridized slightly with Rb *p* and t_{2g} states. These bands lead to an anomalously flat anion *p* band near the Fermi level, as shown in the previous paragraph, and reflect the bonding states. In contrast to the *p*

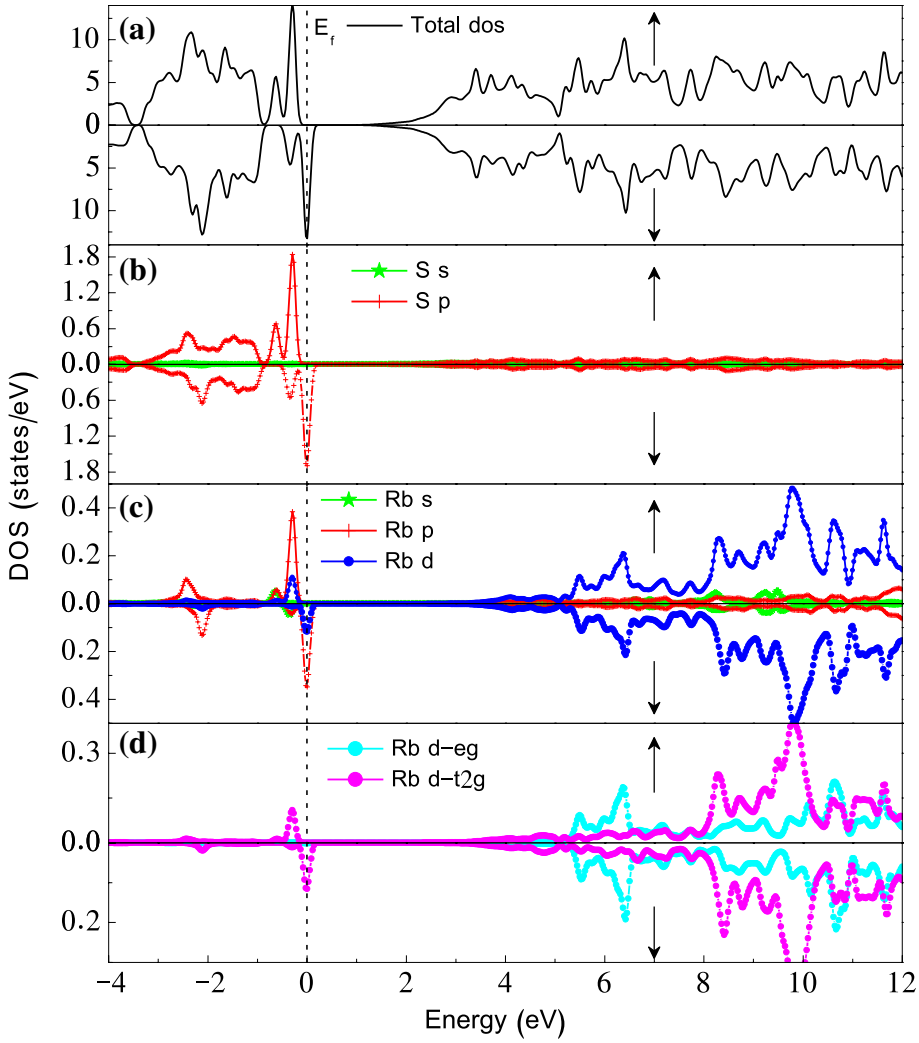

Fig. 6 **a** TDOS and **b–d** PDOS of Rb-doped ZnS. The upwards arrows (downwards arrows) represent the majority (minority) spin directions, and vertical dashed line indicates Fermi level (Color figure online)

states, most of *d* states belonging to e_g and t_{2g} representations are located at higher conduction energies at about 4–16.5 eV. Hence, these states are not directly involved in formation of spin polarization and ferromagnetism in Rb-doped zinc chalcogenides. It was found in previous study that the origin of HM ferromagnetism in alkali-based beryllium perovskites $MBeO_3$ is attributed to the hole mediated double exchange mechanism through the *p* -*p* coupling between M and O atoms [57]. In the present case, the exchange splitting of S-3p/Se-4p states around E_f plays the pivotal role in the appearance of the half-metallicity. Thus the magnetic moment is mainly attributed to the (S, Se)-*p* states, and minor contribution of Rb atom to the total moment results from the hybridization between the (S, Se)-*p* and Rb *p* and Rb t_{2g} states, which is consistent with spin charge density calculation. However, the governing mechanism behind these systems clearly distinguishes them from TM (TM = Mn, Fe, Co, Ni)-doped ZnS/Se [15] where TM *d* electrons provide the main magnetic moment and the *p*-*d* hybridization coupling is responsible for ferromagnetism. We note that in the case of V- and Cr-doped ZnS/Se, the ferromagnetic state is stable via double exchange coupling in which the delocalized antibonding band is partially occupied [50].

4 Conclusion

In conclusion, electronic and ferromagnetic properties of alkali metals (K, Rb and Cs) incorporated ZnS/Se systems have been studied using first-principles calculation. These systems showed 100% spin polarization at Fermi level with gap in the spin-up channel when alkali dopant replaces the Zn site in periodic supercells. The band gap decreases as one goes from K to Cs. In all cases under study, half-metallic ferromagnetism has been observed

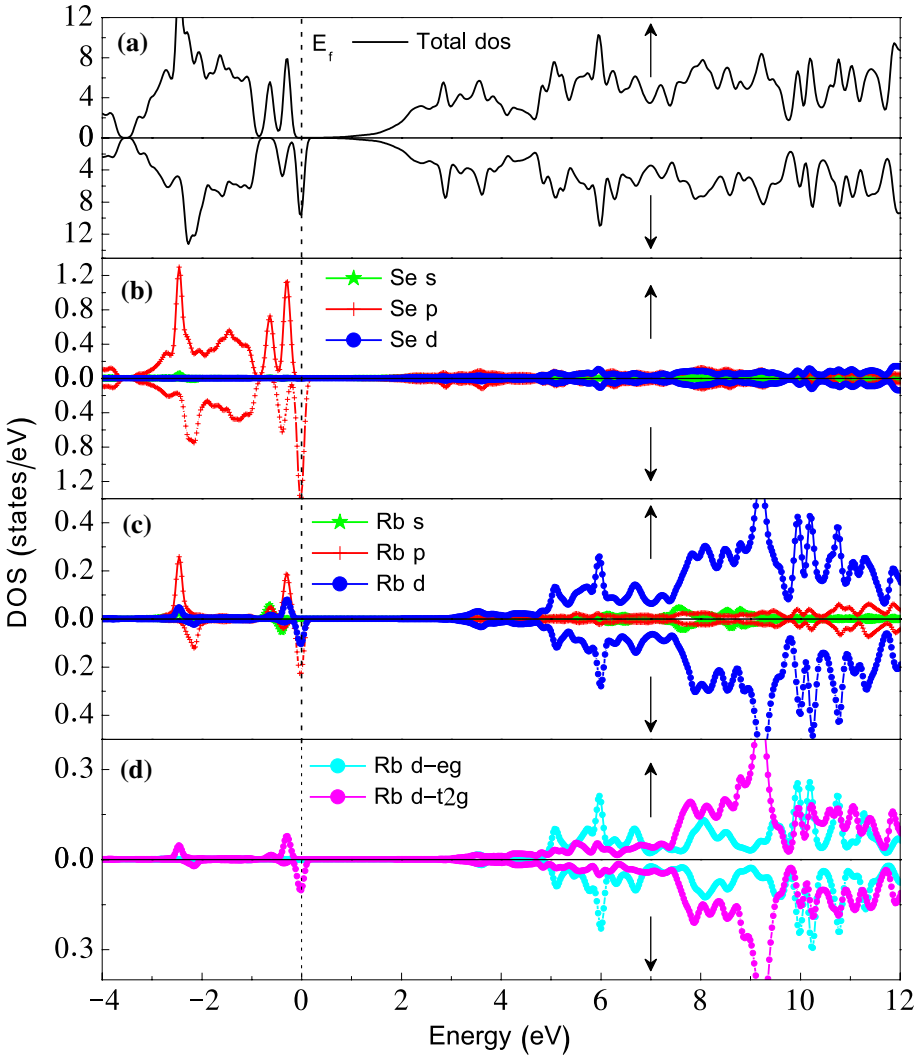

Fig. 7 **a** TDOS and **b–d** PDOS of Rb-doped ZnSe. The upwards arrows (downwards arrows) represent the majority (minority) spin directions, and vertical dashed line indicates Fermi level (Color figure online)

with an induced magnetic moment of 1.00 μ_B per dopant atom leading to minimal energy losses in spintronic applications. From the analysis of partial density of states and magnetic moments, the origin of half-metallicity arises from the spin polarization of the chalcogen *p*-orbitals. Thus alkali metals may be promising non-magnetic dopants for zinc chalcogenides to fabricate dilute magnetic semiconductors free of magnetic precipitates.

Funding The authors have not disclosed any funding.

Data availability Enquiries about data availability should be directed to the authors.

Declarations

Competing interest The authors have not disclosed any competing interest.

References

1. Wolf, S.A., Awschalom, D.D., Buhrman, R.A., Daughton, J.M., von Molnar, S., Roukes, M.L., Chtchelkanova, A.Y., Treger, D.M.: Spintronics: a spin-based electronics vision for the future. Science **294**, 1488–1495 (2001). https://doi.org/10.1126/science.1065389
2. Žutić, I., Fabian, J., Das Sarma, S.: Spintronics: fundamentals and applications. Rev. Mod. Phys. **76**, 323–410 (2004). https://doi.org/10.1103/RevModPhys.76.323
3. Zhang, Y., Liu, W., Niu, H.: Half-metallic ferromagnetism in Cr-doped AlP-density functional calculations. Solid State Commun. **145**, 590–593 (2008). https://doi.org/10.1016/j.ssc.2007.12.022
4. Zhao, Y.-H., Zhao, G.-P., Liu, Y., Liu, B.-G.: Structural stability and half-metallicity of the zinc-blende phase of $Al_{1-x}Cr_xAs$: density-functional study. Phys. Rev. B **80**, 224417 (2009). https://doi.org/10.1103/PhysRevB.80.224417
5. Sajjad, M., Manzoor, S., Zhang, H.X., Noor, N.A., Alay-e-Abbas, S.M., Shaukat, A., Khenata, R.: The half-metallic ferromagnetism character in $Be_{1-x}V_xY$ (Y = Se and Te) alloys: an ab-initio study. J. Magn. Magn. Mater. **379**, 63–73 (2015). https://doi.org/10.1016/j.jmmm.2014.11.004

6. Berber, M., Doumi, B., Mokaddem, A., Mogulkoc, Y., Sayede, A., Tadjer, A.: Investigation of electronic structure and half-metallic ferromagnetic behavior with large half-metallic gap in $Sr_{1-x}V_xO$. J. Comput. Electron **16**, 542–547 (2017). https://doi.org/10.1007/s10825-017-1038-z
7. Dietl, T., Ohno, H., Matsukura, F., Cibert, J., Ferrand, D.: Zener model description of ferromagnetism in zinc-blende magnetic semiconductors. Science **287**, 1019–1022 (2000). https://doi.org/10.1126/science.287.5455.1019
8. Chitta, V.A., Coaquira, J.A.H., Fernandez, J.R.L., Duarte, C.A., Leite, J.R., Schikora, D., As, D.J., Lischka, K., Abramof, E.: Room temperature ferromagnetism in cubic GaN epilayers implanted with Mn^+ ions. Appl. Phys. Lett. **85**, 3777–3779 (2004). https://doi.org/10.1063/1.1812590
9. Liu, H.X., Wu, S.Y., Singh, R.K., Gu, L., Smith, D.J., Newman, N., Dilley, N.R., Montes, L., Simmonds, M.B.: Observation of ferromagnetism above 900 K in Cr– GaN and Cr–AlN Appl. Phys. Lett. **85**, 4076–4078 (2004). https://doi.org/10.1063/1.1812581
10. Sato, K., Dederics, P.H., Katayama-Yoshida, H.: Curie temperatures of III–V diluted magnetic semiconductors calculated from first principles. Europhys. Lett. **61**, 403–408 (2003). https://doi.org/10.1209/epl/i2003-00191-8
11. Granville, S., Ruck, B.J., Preston, A.R.H., Stewart, T., Budde, F., Trodahl, H.J., Bittar, A., Downes, J.E., Ridgway, M.: Electronic properties of (Ga, Mn)N thin films with high Mn content. J. Appl. Phys. **104**, 103710 (2008). https://doi.org/10.1063/1.3020536
12. Singh, J., Kumar, S., Verma, N.K.: Enhancement of room temperature ferromagnetism in $Cd_{1-x}Ni_xSe$ nanoparticles. J. Mater. Sci. Mater. Electron **25**, 2267–2272 (2014). https://doi.org/10.1007/s10854-014-1870-x
13. Fang, W., Liu, Y., Guo, B., Peng, L., Zhong, Y., Zhang, J., Zhao, Z.: Room temperature ferromagnetism and cooling effect in dilute Co-doped ZnS nanoparticles with zinc blende structure. J. Alloys Compd. **584**, 240–243 (2014). https://doi.org/10.1016/j.jallcom.2013.08.215
14. Akhtar, M.S., Malik, M.A., Alghamdi, Y.G., Ahmad, K.S., Riaz, S., Naseem, S.: Chemical bath deposition of Fe-doped ZnS thin films: investigations of their ferromagnetic and half-metallic properties. Mater. Sci. Semicond. Process. **39**, 283–291 (2015). https://doi.org/10.1016/j.mssp.2015.05.017
15. Mahmood, Q., Hassan, M., Noor, N.A.: Systematic study of room-temperature ferromagnetism and the optical response of $Zn_{1-x}TM_xS/Se$ (TM = Mn, Fe Co, Ni) ferromagnets: first-principle approach. J. Phys. Condens. Matter **28**, 506001 (2016)
16. Sato, K., Katayama-Yoshida, H.: Ab initio study on the magnetism in ZnO-, ZnS-, ZnSe- and ZnTe-based diluted magnetic semiconductors. Phys. Stat. Sol. B **229**, 673–680 (2002). https://doi.org/10.1002/1521-3951(200201)229:2%3c673::AID-PSSB673%3e3.0.CO;2-7
17. Sambasivam, S., Joseph, D.P., Reddy, D.R., Reddy, B.K., Jayasankar, C.K.: Synthesis and characterization of thiophenol passivated Fe-doped ZnS nanoparticles. Mater. Sci. Eng. B **150**, 125–129 (2008). https://doi.org/10.1016/j.mseb.2008.03.009
18. Sambasivam, S., Joseph, D.P., Lin, J.G., Venkateswaran, C.: Doping induced magnetism in Co–ZnS nanoparticles. J. Solid State Chem. **182**, 2598–2601 (2009). https://doi.org/10.1016/j.jssc.2009.07.015
19. Lakshmi, P.V.B., Raj, K.S., Ramachandran, K.: Synthesis and characterization of nano ZnS doped with Mn. Cryst. Res. Tech. **44**, 153–158 (2009). https://doi.org/10.1002/crat.200800271
20. Ahmed, S.A.: Room-temperature ferromagnetism in Co-, Cr-, and V-doped ZnO diluted magnetic semiconductor. Appl. Phys. A **123**, 440 (2017). https://doi.org/10.1007/s00339-017-1058-3
21. Soundararajan, D., Mangalaraj, D., Nataraj, D., Dorosinskii, L., Kim, K.H.: Magnetic properties of Cr doped ZnTe alloy powder. Mater. Lett. **87**, 113–116 (2012). https://doi.org/10.1016/j.matlet.2012.07.042
22. Hou, X.J., Teo, K.L., Sreenivasan, M.G., Liew, T., Chong, T.C.: MBE growth and properties of Cr-doped ZnTe on GaAs(001). Thin Solid Films **505**, 126–128 (2006). https://doi.org/10.1016/j.tsf.2005.10.024
23. Park, J.H., Kim, M.G., Jang, H.M., Ryu, S., Kim, Y.M.: Co-metal clustering as the origin of ferromagnetism in Co-doped ZnO thin films. Appl. Phys. Lett. **84**, 1338–1340 (2004). https://doi.org/10.1063/1.1650915
24. Kaspar, T.C., Droubay, T., Heald, S.M., Engelhard, M.H., Nachimuthu, P., Chambers, S.A.: Hidden ferromagnetic secondary phases in cobalt-doped ZnO epitaxial thin films. Phys. Rev. B **77**, 201303 (2008). https://doi.org/10.1103/PhysRevB.77.201303
25. Zheng, F.-B., Zhang, C.-W., Wang, P.-J., Luan, H.-X.: Tuning the electronic and magnetic properties of carbon-doped ZnO nanosheets: first-principles prediction. J. Appl. Phys. **111**, 044329 (2012). https://doi.org/10.1063/1.3688233
26. Pan, H., Feng, Y.P., Wu, Q.Y., Huang, Z.G., Lin, J.: Magnetic properties of carbon doped CdS: a first-principles and Monte Carlo study. Phys. Rev. B **77**, 125211 (2008). https://doi.org/10.1103/PhysRevB.77.125211
27. Hua, P., Sha, Z., Shen, L.F.: Electronic structures and magnetic couplings of B-, C-, and N-doped BeO. Chin. Phys. B **22**, 047504 (2013). https://doi.org/10.1088/1674-1056/22/4/047504
28. Kenmochi, K., Seike, M., Sato, K., Yanase, A., Katayama-Yoshida, H.: New class of diluted ferromagnetic semiconductors based on CaO without transition metal elements Jpn. J. Appl. Phys. **43**, L934–L936 (2004). https://doi.org/10.1143/JJAP.43.L934
29. Kang, B.-S., Kim, K.-S., Yu, S.-C., Chae, H.: First-principles study for ferromagnetism of Cu-doped ZnO with carrier doping. J. Solid State Chem. **198**, 120–124 (2013). https://doi.org/10.1016/j.jssc.2012.09.041
30. Adli, W.: Prediction of half-metallic ferromagnetism in Cu- and K-doped MgS: a comparative study. J. Supercond. Novel. Magn. **33**, 3107–3112 (2020). https://doi.org/10.1007/s10948-020-05558-3
31. Khan, Z.A., Ghosh, S.: Robust room temperature ferromagnetism in Cu doped ZnO thin films. Appl. Phys. Lett. **99**, 042504 (2011). https://doi.org/10.1063/1.3615714
32. Yu, C.-F., Lin, T.-J., Sun, S.-J., Chou, H.: Origin of ferromagnetism in nitrogen embedded ZnO : N thin films. J. Phys. D: Appl. Phys. **40**, 6497–6500 (2007). https://doi.org/10.1088/0022-3727/40/21/004
33. Zhou, S., Xu, Q., Potzger, K., Talut, G., Grötzschel, R., Fassbender, J., Vinnichenko, M., Grenzer, J., Helm, M., Hochmuth, H., Lorenz, M., Grundmann, M., Schmidt, H.: Room temperature ferromagnetism in carbon-implanted ZnO. Appl. Phys. Lett. **93**, 232507 (2008). https://doi.org/10.1063/1.3048076
34. Saravanan, N., Teh, G.B., Yap, S.Y.P., Cheong, K.M.: Simple synthesis of ZnS nanoparticles in alkaline medium. J. Mater. Sci. Mater. Electron. **19**, 1206–1208 (2008). https://doi.org/10.1007/s10854-007-9529-5
35. Fang, X., Bando, Y., Gautam, U.K., Zhai, T., Zeng, H., Xu, X., Liao, M., Golberg, D.: ZnO and ZnS nanostructures: ultraviolet-light emitters, lasers, and sensors. Crit. Rev. Solid State Mater. Sci **34**, 190–223 (2009). https://doi.org/10.1080/10408430903245393
36. Samadpour, M., Dehghani, M., Parand, P., Najafi, M.N., Parvazian, E.: Photovoltaic performance and electrochemical impedance spectroscopy analysis of CdS/CdSe- sensitized solar cell based on surfactant-modified ZnS treatment. Appl. Phys. A **126**, 461 (2020). https://doi.org/10.1007/s00339-020-03652-w
37. Wang, X., Xie, Z., Huang, H., Liu, Z., Chen, D., Shen, G.: Gas sensors, thermistor and photodetector based on ZnS nanowires.

J. Mater. Chem. **22**, 6845–6850 (2012). https://doi.org/10.1039/C2JM16523F
38. Zhao, Q., Xie, Y., Zhang, Z., Bai, X.: Size-selective synthesis of zinc sulfide hierarchical structures and their photocatalytic activity. Cryst. Growth Des. **7**, 153–158 (2007). https://doi.org/10.1021/cg060521j
39. Holzman, J.F., Vermeulen, F.E., Irvine, S.E., Elezzabi, A.Y.: Free-space detection of terahertz radiation using crystalline and polycrystalline ZnSe electro-optic sensors. Appl. Phys. Lett. **81**, 2294–2296 (2002). https://doi.org/10.1063/1.1508435
40. Zhang, C.-W., Yan, S.-S.: First-principles prediction of half-metallic ferromagnetism in Cu-doped ZnS. J. Appl. Phys. **107**, 043913 (2010). https://doi.org/10.1063/1.3309771
41. Long, R., English, N.J.: Magnetic properties of first-row element-doped ZnS semiconductors: a density functional theory investigation. Phys. Rev. B **80**, 115212 (2009). https://doi.org/10.1103/PhysRevB.80.115212
42. Blaha, P., Schwarz, K., Madsen, G.K.H., Kvasnicka, D., Luitz, J.: Wien2k, an augmented plane wave program for Calculating crystal properties. Vienna University of Technology, Vienna (2001)
43. Hohenberg, P., Kohn, W.: Inhomogeneous electron gas. Phys. Rev. **136**, B864–B871 (1964). https://doi.org/10.1103/PhysRev.136.B864
44. Perdew, J.P., Burke, K., Ernzerhof, M.: Generalized gradient approximation made simple. Phys. Rev. Lett. **77**, 3865–3868 (1996). https://doi.org/10.1103/PhysRevLett.77.3865
45. Monkhorst, H.J., Pack, J.D.: Special points for Brillouin-zone integrations. Phys. Rev. B **13**, 5188 (1976). https://doi.org/10.1103/PhysRevB.13.5188
46. Murnaghan, F.D.: The compressibility of media under extreme pressures. Proc. Nat. Acad. Sci. U.S.A. **30**, 244–247 (1944). https://doi.org/10.1073/pnas.30.9.244
47. Fan, S.W., Dong, J.H., Ding, L.J., Wang, Z.L., Yao, K.L.: Half-metallic ferromagnetism in tetrahedrally coordinated compounds MGe (M = Ca, Sr and Ba): Ab initio calculations. Comput. Mater. Sci. **67**, 83–87 (2013). https://doi.org/10.1016/j.commatsci.2012.08.026
48. Gao, G.Y., Yao, K.L.: Half-metallic sp-electron ferromagnets in rocksalt structure: the case of SrC and BaC. Appl. Phys. Lett. **91**, 082512 (2007). https://doi.org/10.1063/1.2775081
49. Yao, K.L., Gao, G.Y., Liu, Z.L., Zhu, L.: Half-metallic ferromagnetism of zinc-blende CrS and CrP: a first-principles pseudopotential study. Solid State Commun. **133**, 301–304 (2005). https://doi.org/10.1016/j.ssc.2004.11.016
50. Sato, K., Katayama-Yoshida, H.: Materials design of transparent and half-metallic ferromagnets in V- or Cr-doped ZnS, ZnSe and ZnTe without P- or N-type doping treatment. Jpn. J. Appl. Phys. **40**, L651–L653 (2001). https://doi.org/10.1143/JJAP.40.L651
51. Yao, K.L., Jiang, J.L., Liu, Z.L., Gao, G.Y.: First principle prediction of half-metallic ferromagnetism in zinc-blende MBi (Ca, Sr, Ba). Phys. Lett. A. **359**, 326–329 (2006). https://doi.org/10.1016/j.physleta.2006.06.052
52. Sieberer, M., Redinger, J., Khmelevskyi, S., Mohn, P.: Ferromagnetism in tetrahedrally coordinated compounds of I/II-V elements: Ab initio calculations. Phys. Rev. B. **73**, 024404 (2006). https://doi.org/10.1103/PhysRevB.73.024404
53. Kanamori, J., Terakura, K.: A general mechanism underlying ferromagnetism in transition metal compounds. J. Phys. Soc. Jpn. **70**, 1433–1434 (2001). https://doi.org/10.1143/jpsj.70.1433
54. Krstajić, P.M., Peeters, F.M., Ivanov, V.A., Fleurov, V., Kikoin, K.: Double-exchange mechanisms for Mn-doped III-V ferromagnetic semiconductors. Phys. Rev. B **70**, 195215 (2004). https://doi.org/10.1103/PhysRevB.70.195215
55. Liu, H., Zhang, J.-M.: Effect of two identical 3d transition-metal atoms M doping (M = V, Cr, Mn, Fe Co, and Ni) on the structural, electronic, and magnetic properties of ZnO Phys. Status Solidi B **254**, 1700098 (2017). https://doi.org/10.1002/pssb.201700098
56. Chen, W.Q., Teo, K.L., Lim, S.T., Jalil, M.B.A., Liew, T., Chong, T.C.: Magnetic and transport behaviors in $Ge_{1-x}Mn_xTe$ with high Mn composition. Appl. Phys. Lett. **90**, 142514 (2007). https://doi.org/10.1063/1.2720353
57. Mahmood, Q., Ul Haq, B., Yaseen, M., Shahid, A., Laref, A.: Exploring the origin of p- type half-metallic ferromagnetism in beryllium doped alkali based perovskites. Solid State Commun. **299**, 113654 (2019). https://doi.org/10.1016/j.ssc.2019.113654